Tectonics®

RESEARCH ARTICLE
10.1029/2021TC007086

Key Points:

- The relative pace of slab-pull force build-up and overriding plate weakening has a crucial role in setting the style of back-arc rifting
- Our slowly converging subduction model with narrow oceanic basin and weak back-arc reproduce first order features of the Pannonian basin

Supporting Information:

Supporting Information may be found in the online version of this article.

Correspondence to:

Z. Erdős,
zoltan-erdos@staff.elte.hu

Citation:

Erdős, Z., Huismans, R. S., & Faccenna, C. (2022). Wide versus narrow back-arc rifting: Control of subduction velocity and convective back-arc thinning. *Tectonics*, *41*, e2021TC007086. https://doi.org/10.1029/2021TC007086

Received 27 SEP 2021
Accepted 21 MAY 2022

Wide Versus Narrow Back-Arc Rifting: Control of Subduction Velocity and Convective Back-Arc Thinning

Zoltán Erdős[1,2], Ritske S. Huismans[3], and Claudio Faccenna[4,5]

[1]Institute of Earth Physics and Space Science, ELKH, Sopron, Hungary, [2]Department of Geophysics and Space Science, Institute of Geography and Earth Sciences, ELTE Eötvös Loránd University, Budapest, Hungary, [3]Department of Earth Sciences, University of Bergen, Bergen, Norway, [4]Department of Science, University Roma Tre, Roma, Italy, [5]GFZ Potsdam, Potsdam, Germany

Abstract Back-arc basins such as the ones behind the island-arcs of the Western Pacific Ocean or the ones in the Mediterranean Sea are ubiquitous structures of the Earth. They are extensional basins forming in the overriding plate behind subduction zones and similarly to continental rifts, they can exhibit different structural styles from narrow, localized rifting to wide-rift extension. While these different structural styles have been long recognized, the factors controlling the style of extension in these basins have not been explored properly. We use thermo-mechanical models to investigate how the relative rates of progressive build-up of slab-pull force and of convective thinning and thermal weakening of the overriding plate control the style of back-arc rifting. Following subduction-initiation, a high subducting plate velocity results in rapid build-up of the slab-pull force. The relatively low rate of convectively thinning and associated moderate weakening of the overriding plate require slab-pull to build up to close to its maximum value to overcome the high back-arc integrated strength resulting in a narrow back-arc rift. In turn a low subducting plate velocity in comparison with the timescale of convective thinning of the overriding plate allows for significant back-arc weakening before the slab-pull force becomes large enough to drive back-arc extension. In this case, the back-arc exhibits a wide rifting style as extension occurs at significantly reduced overriding plate integrated strength. Our model results provide an explanation why some subduction zones exhibit wide, distributed extension in the overriding plate such as for instance observed in the Pannonian basin.

1. Introduction

Back-arc basins are extensional basins that form behind subduction zones in the overriding plate (Taylor & Karner, 1983). They form in both ocean-ocean or ocean-continent subduction settings and exhibit a wide range of features from narrow, symmetrical back-arc rifts to widespread extension for hundreds of kilometers behind the arc (e.g., Faccenna et al., 1997; Jolivet et al., 1999; Tamaki, 1985). Many back-arc basins, especially in the Circum-Pacific region are the result of narrow, localized rifting and crustal breakup, such as for instance the Okinawa trough behind the Ryukyu arc (e.g., Qi et al., 2021; Sibuet et al., 1987, 1998; Zhang et al., 2021). These basins often form behind Pacific subduction zones where convergence rates are high (e.g., Faccenna et al., 2007; Heuret & Lallemand, 2005; Heuret et al., 2007; Sdrolias & Müller, 2006; see also Figure 1 in Schellart et al. [2007]). In contrast, other back-arc basins, especially in the Mediterranean region where deformation is driven by the slow convergence between Eurasia and Africa (Faccenna et al., 2014), exhibit wide rifting, as for instance the Pannonian basin (Figure 1; Bada et al., 1999; Balázs et al., 2017; Csontos et al., 1992; Horváth et al., 2006). Despite the relative abundance of back-arc basins around the globe, systematic modeling studies focusing on their dynamics and on factors controlling their style of extension are rare, compared to the abundance of studies focusing on the simpler case of continental rifting.

Common parameters that may influence the style of simple continental rifts include the thermal and rheological structure of the lithosphere, the rate of extension, inherited crustal weaknesses, and magmatic intrusions (e.g., Balázs et al., 2017; Brun, 1999; Buck, 1991; Buck et al., 1999; Buiter et al., 2008; Burov, 2007; Burov & Poliakov, 2001; Huismans & Beaumont, 2003, 2011; Liao & Gerya, 2014). It was shown early on, that out of these parameters crustal thickness, heat flow, and strain-rate are factors controlling the mode of extension (Buck, 1991). Weak lithosphere, thick crust and low strain-rate tend to favor wide rifting, while strong, cold lithosphere and high strain-rate promote narrow, localized rifting (Buck, 1991). The modeling experiments of Bassi (1995) indicated that low strain-rate (extension rate) is important, but not enough to produce a wide rift,

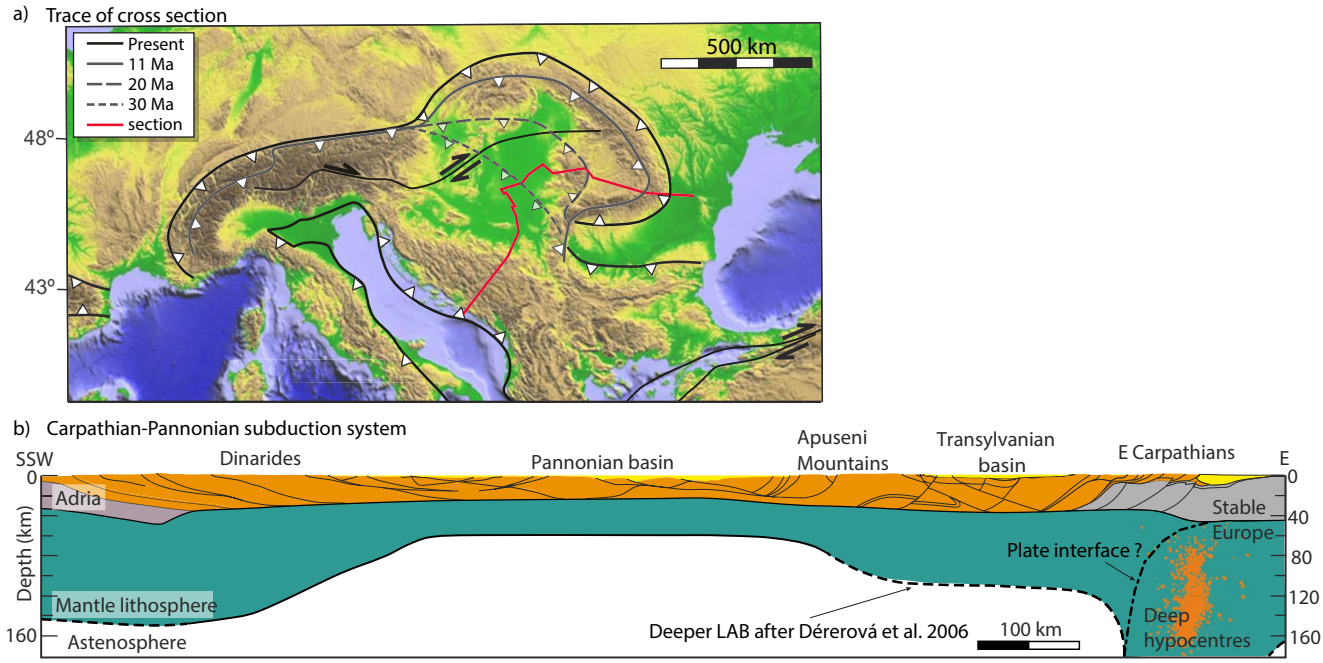

Figure 1. (a) Simplified tectonic outlines of plate contacts in the Carpathian-Pannonian region (after Faccenna et al. [2014] and Schmid et al. [2008]). Dashed black lines show the positions of the orogenic front prior to the onset of extension in back-arc basins (modified after Wortel and Spakman [2000]). Sa—Sava Suture Zone (b) Lithospheric scale cross-section over the Dinarides–Pannonian Basin–Apuseni Mountains–Transylvanian Basin–East Carpathians (compiled from Balázs et al. [2016], Matenco et al. [2016], and Schmid et al. [2008]). The dashed LAB portion is taken after Dérerová et al. (2006). The trace of the cross section was chosen to approximate the curved North to North-East to East direction of extension accompanying the clockwise rotation of the Tisza-Dacia unit.

and emphasizes the role of a rheologically weak mantle lithosphere. Huismans and Beaumont (2008, 2011) have shown that the style of rifting and that of the evolving passive margins is largely controlled by crust and mantle rheology. High crustal and mantle lithospheric strength leads to strong coupling between these layers and narrow necking, while low crustal strength results in differential thinning and wide, distributed rifting.

In case of back-arc rifting, where extension occurs in close proximity to an active subduction zone, additional controlling factors include the rate of trench-retreat (partly controlled by relative plate motions and the age of the oceanic lithosphere), the pattern of asthenospheric flow in three dimensions, the absolute plate motions, and the long term strength of the subduction interface (Behr & Becker, 2018; Chen et al., 2015; Currie et al., 2008; Funiciello et al., 2003; Király et al., 2016; Magni et al., 2014; Schellart & Moresi, 2013; Schellart et al., 2007; Sdrolias & Müller, 2006; Sheng et al., 2018; Wolf & Huismans, 2019). Moreover, for back-arc rifts both the rate of extension and the rheological setup of the overriding plate (two main controlling factors for continental rifts) are externally controlled factors. The extension-rate is controlled by the dynamics of the nearby subduction zone through the dynamic build-up of slab-pull force as well as the absolute plate motions. A wealth of analogue models have focused on the effects of overriding plate and subducting plate velocities on the deformation style of the back-arc zone (e.g., Chen et al., 2015; Heuret & Lallemand, 2005; Heuret et al., 2007). However, these models mainly used overriding plate rheologies that were constant throughout the modeling experiments. In contrast, the thermal and rheological structure of the overriding plate might evolve over time owing to re-hydration or convective removal of the lithospheric mantle (e.g., Arcay et al., 2005, 2006; Gerya & Meilick, 2011). Wolf and Huismans (2019) concluded using a force-balance analysis that the driving and resisting forces acting on the overriding plate lithosphere are in a near equilibrium state during subduction and that overriding plate weakening is necessary for back-arc extension to occur. This result is in good agreement with the early analogue experimental results of Shemenda (1993). The numerical modeling results of Wolf and Huismans (2019) suggest that convective removal of weak overriding plate mantle lithosphere plays a primary role in weakening and the initiation of back-arc extension.

Here we use numerical thermo-mechanical model experiments to investigate factors controlling the style of back-arc extension with a special focus on the combined effects of subducting plate velocity (i.e., the far-field velocity of the subducting plate relative to the undeforming part of the overriding plate) and convective thinning of the back-arc mantle lithosphere. The subducting plate velocity varies widely in nature and exerts a first order control on the build-up of the slab-pull force following subduction initiation.

2. Numerical Method

2.1. Model Description

We use a modified version of the 2D finite element numerical modeling code FANTOM (Thieulot, 2011; Wolf & Huismans, 2019) to model subduction and simultaneous back-arc extension. The numerical experimental setup is very similar to the one used in our previous studies (e.g., Erdős et al., 2021; Wolf & Huismans, 2019) and is described in detail of Supporting Information S1. FANTOM is designed to solve the Stokes equation coupled to the heat transport equation in 2D using the plane strain assumption. The thermo-mechanical model consists of strain-weakening frictional plastic and thermally activated non-linear viscous creep materials (see Table 1 for material properties).

2.2. Initial Experimental Setup and Boundary Conditions

The experimental setup includes a computational model domain that is 1,400 km deep and 3,000 km wide (Figure 2). The initial layered geometry consists of a constant viscosity lower mantle overlain by an adiabatic sub-lithospheric mantle that has a rheology of wet olivine (Karato & Wu, 1993). Above these two layers, the setup varies depending on the type of lithosphere. The right side of the model consists of the overriding continental lithospheric plate with an 84 km thick mantle lithosphere (wet olivine with a scaling factor 5 for the strong, distal portion and a scaling factor of 0.2 for the weak, proximal portion), a 12 km thick lower crust (dry Maryland diabase with a scaling factor of 0.1; Mackwell et al., 1998), a 20 km thick upper crust (wet quartz with a scaling factor of 1) and a 4 km thick sedimentary cover (wet quartz with a scaling factor of 1; Gleason & Tullis, 1995).

The left side of the model consists of oceanic lithosphere, with 71 km thick oceanic mantle lithosphere (wet olivine with a scaling factor of 5) and 9 km thick oceanic crust (dry Maryland diabase with a scaling factor of 0.1). The upper 60 km of the oceanic mantle lithosphere is depleted by 15 kgm^{-3}. The boundary between these two blocks is dipping 35° to the right. At this divide, the model is seeded with an inclined, strain-weakened oceanic crustal domain underneath the overriding plate to allow for oceanic subduction initiation. A pro-continental lithospheric block trailing the subducting oceanic lithosphere is only present in models 3 and 4. In these models, the oceanic lithosphere is bounded on the left by a narrow, steeply dipping passive continental margin. The trailing continental lithosphere consists of a 24 km thick upper crust, a 12 km thick lower crust and an 84 km thick continental lithospheric mantle. The continent to the left has a similar rheological setup to the overriding plate but there is no sedimentary cover and the upper crust has a rheology of wet quartz with a scaling factor of 5. We have adjusted the strength of this domain in order to prevent the front-end of the incoming continent from being wrenched off by the fully subducted slab. All material properties are listed in Table 1. We use a scaling factor (f) to approximate the effect of variations in volatile content and potential changes in strength owing to compositional variations (Beaumont et al., 2006). Upon reaching the temperature-pressure phase-change boundary conditions the oceanic crust is transformed into eclogite (Hacker, 1996). Eclogite has the same viscous flow law as the oceanic crust but a different density (see Table 1). All slab and mantle materials are subject to a reversible phase transition at the 660 km discontinuity, corresponding to the breakdown of ringwoodite to bridgmanite and magnesiowüstite (see discussion in Billen [2010] and Goes et al. [2017]). For simplicity, all materials that make up the subducting slab are converted to one lower mantle slab material with the viscous flow law of the oceanic lithosphere. The phase changes do not account for latent heat and are not mass conserving but are assumed to capture the first-order effects of important metamorphic phase changes (Wolf & Huismans, 2019).

The viscosity of the iso-viscous lower mantle used in this study is consistent with the viscosity structure of the mantle inferred from inversion studies (e.g., Billen, 2010; Mitrovica & Forte, 2004). The higher viscosity of the lower mantle (relative to the sub-lithospheric upper mantle; see Figure S1 for the density and viscosity structure

Tectonics
10.1029/2021TC007086

Table 1
Material Properties

	Materials										
		Continental plate			Oceanic plate				Asthenosphere		
Units	Sedimentary cover	Upper crust (pro)	Lower crust	Mantle lithosphere	Crust	Mantle lithosphere	Eclogite from sediment	Eclogite from crust	Sublithospheric mantle	Constant viscosity lower mantle	Slab in the lower mantle
					Mechanical parameters						
Thickness (km)	4	24	12	84	9	71	-	-	536 (580)[a]	740	-
Reference density (kg m^{-3})	2,800	2,800	3,000	3,380 (3,360)[b]	2,900	3,380 (3,365)[c]	3,365	3,380	3,380	3,630	3,630
Friction angle (deg)	8–2°	15–2°	15–2°	15–2°	7–1°	15–2°	15–2°	15–2°	15–2°	-	15–2°
Cohesion (Pa)	2×10^7–4×10^6	2×10^7	2×10^7	2×10^7	2×10^7	2×10^7	2×10^7–4×10^6	2×10^7	2×10^7	-	2×10^7
Flow law	WQ[1]	WQ[1]	DMD[2]	WO[3]	DMD[2]	WO[3]	WQ[1]	DMD[2]	WO[3]	-	WO[3]
scaling factor	1	1 (5)[d]	0.1	5 (0.2)[e]	0.1	5	0.5	0.1	1	-	5
A (Pa^{-n} s^{-1})	8.574×10^{-28}	8.574×10^{-28}	5.78×10^{-27}	1.76×10^{-14}	5.78×10^{-27}	1.76×10^{-14}	8.574×10^{-28}	5.78×10^{-27}	1.76×10^{-14}	-	1.76×10^{-14}
Q (J mol^{-1})	2.228×10^5	2.228×10^5	4.85×10^5	4.3×10^5	4.85×10^5	4.3×10^5	2.228×10^5	4.85×10^5	4.3×10^5	-	4.3×10^5
n	4	4	4.7	3	4.7	3	4	4.7	3	-	3
V (m^3 mol^{-1})	0	0	0	1.1×10^{-5}	0	1.1×10^{-5}	0	0	1.1×10^{-5}	-	1.1×10^{-5}
					Thermal parameters						
Heat capacity (m^2 K^{-1} s^{-2})	750	750	750	1,250	750	1,250	750	750	1,250	1,250	1,250
Heat conductivity (W m^{-1} K^{-1})	2.25	2.25	2.25	2.25	2.25	2.25	2.25	2.25	2.25–52.0	2.25–52.0	2.25
Thermal expansion (K^{-1})	3×10^{-5}	3×10^{-5}	3×10^{-5}	3×10^{-5}–4 10^{-5}	3×10^{-5}	3×10^{-5}–4×10^{-5}	3×10^{-5}	3×10^{-5}	3×10^{-5}–4×10^{-5}	3×10^{-5}–4×10^{-5}	3×10^{-5}–4×10^{-5}
Heat productivity (μW m^{-3})	1.1×10^{-6}	1.1×10^{-6}	5×10^{-7}	0	0	0	0	0	0	0	0
Viscosity range					10^{19}–10^{27}					2×10^{21}	10^{19}–10^{27}

Note. WQ, wet quartz flow-law described by Gleason and Tullis (1995); DMD, dry Maryland diabase flow-law described by Mackwell et al. (1998); WO, wet olivine flow-law described by Karato and Wu (1993).

[a]Value in parenthesis shows the thickness of the sublithospheric mantle under the undeformed oceanic lithosphere. [b]Value in parenthesis shows the density of the depleted layer of continental mantle lithosphere. [c]Value in parenthesis shows the density of the depleted layer of oceanic mantle lithosphere. [d]Value in parenthesis shows the value of the scaling factor applied for the pro-continental upper crust (see text for details). [e]Value in parenthesis shows the scaling factor applied for the weakened portion of the continental mantle lithosphere.

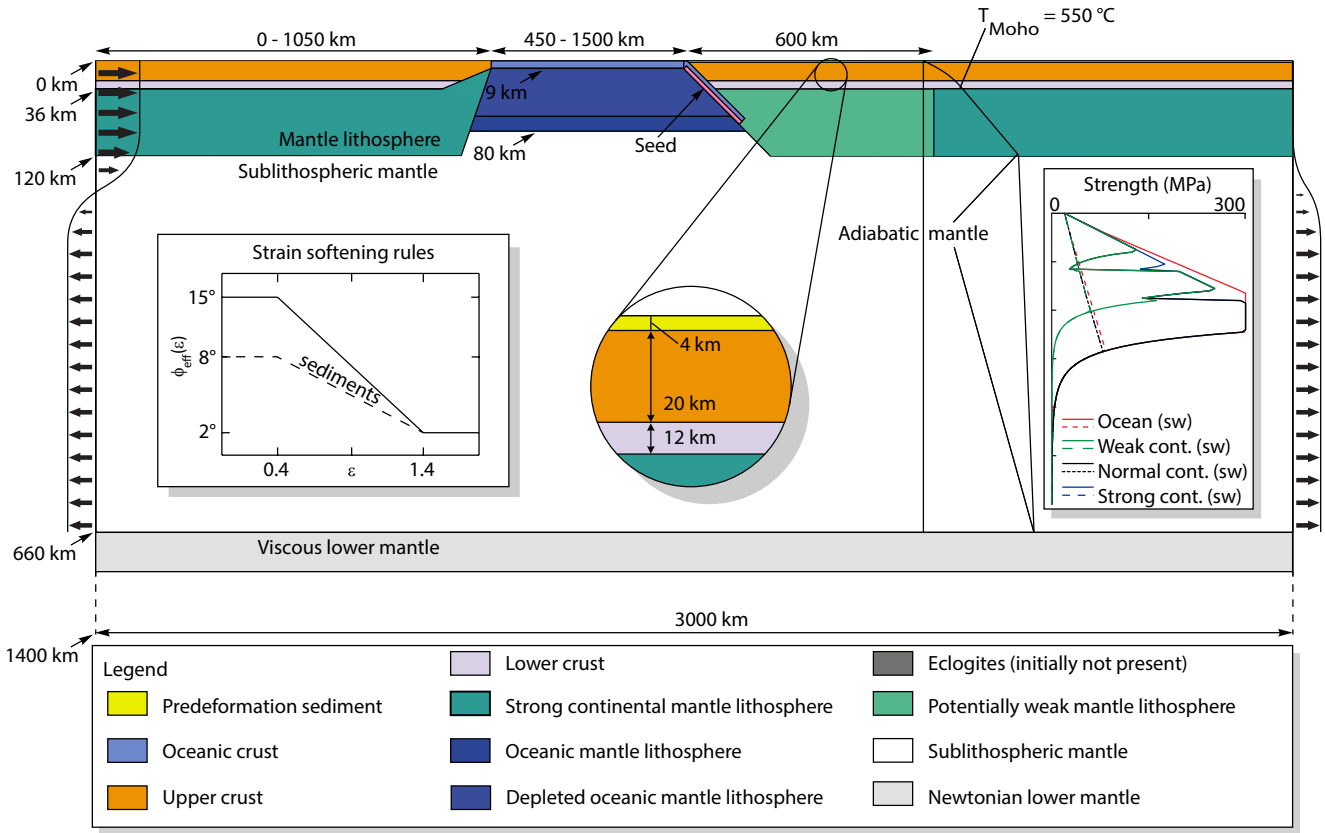

Figure 2. Numerical model design, showing (a) the experimental layout, (b) the velocity boundary conditions, (c) the strain softening rules, (d) the initial temperature field, and (e) the initial strength profiles. The legend identifies the different material types used. For the material properties, of each material type, see Table 1.

of model 1) results in more shear resistance and hence lower sinking velocity for the slab. The shear resistance and the pull of the slab in the lower mantle have a similar magnitude.

The Eulerian computational grid consists of 1,250 cells in the horizontal direction (giving a resolution of 2.4 km) and 257 cells in the vertical direction. The vertical resolution is irregular, with 127 elements covering the bottom 1,270 km of the model (giving a vertical resolution of 10 km), while the remaining 130 elements located in the top 130 km of the model (giving a vertical resolution of 1 km). Grid refinement was used to increase the resolution in the lithosphere, while retaining a reasonable computation time.

The initial temperature field for the continental domain increases with depth from the surface (T_0 = 0°C) to the base of the continental crust (T_m = 550°C), and to the base of the lithosphere (T_{lab} = 1330°C) from where it adiabatically increases to the base of the model domain (T_{base} = 1850°C; see the initial temperature profile on Figure 2). The initial temperature field of the oceanic domain is very similar but the lack of heat-production in the oceanic crust results in a linear geothermal gradient. The bottom and surface boundaries are kept at a constant temperature while the side boundaries are thermally insulated.

Velocity boundary conditions are imposed on both sides of the model with a constant convergence velocity (v_{conv} = 5 cm·yr^{-1} for Model 1 and v_{conv} = 1 cm·yr^{-1} for Models 2–4) imposed on the topmost 120 km of the left side of the model while the right side is kept fixed. For models 3 and 4, where there is a trailing continental lithospheric block present, v_{conv} = 0 cm·yr^{-1} is set after the oceanic basin is fully consumed. The setup of these latter models is designed to mimic the soft docking behavior of small land locked ocean basins such as the precursor to the Pannonian basin—East Carpathian subduction system (e.g., Linzer et al., 1998; Sperner et al., 2002).

The velocity boundary conditions between 120 and 660 km depth are defined so that the material influx and outflux through the lateral boundaries is in balance at any given time. In the constant viscosity lower mantle,

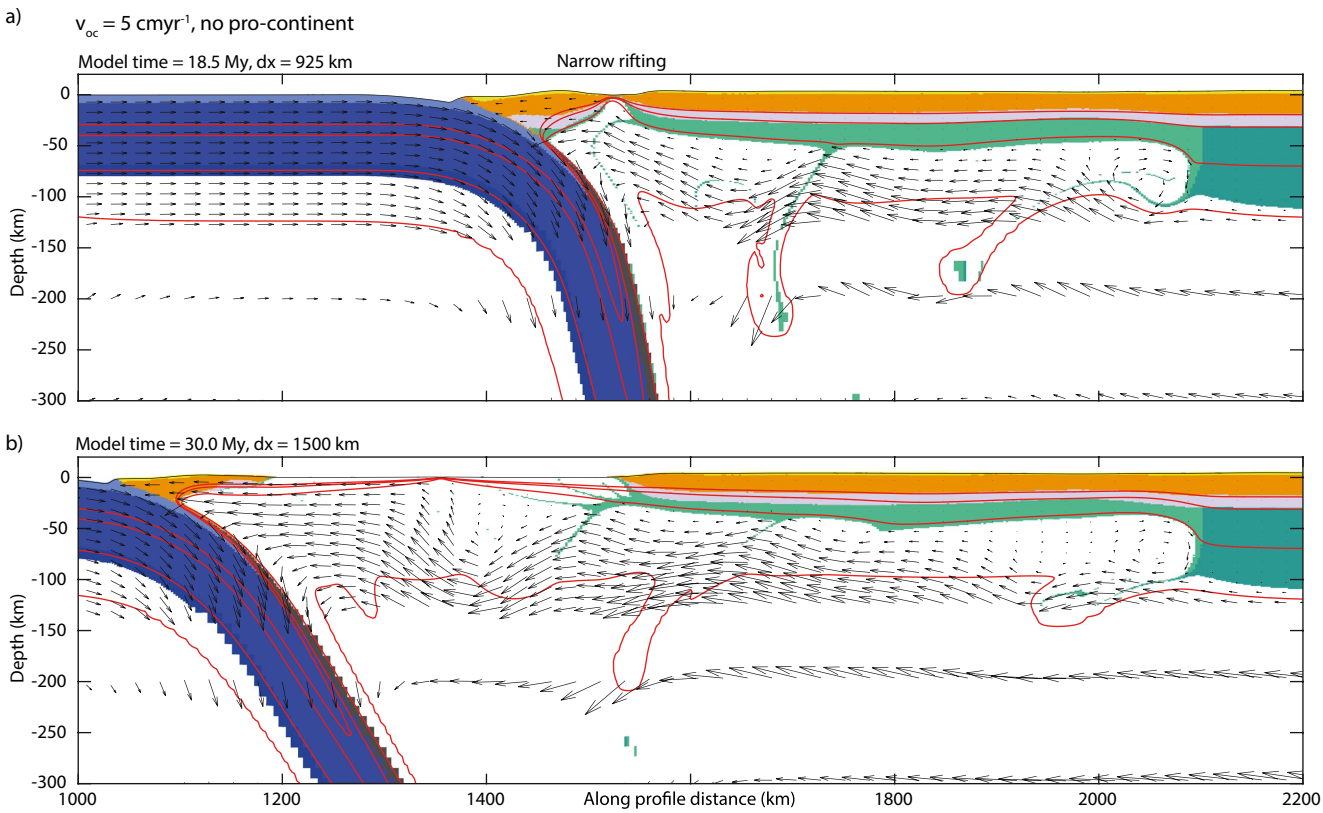

Figure 3. Results of Model 1. Panels (a and b) show zoomed-in images of the experiment's material domain at key time-steps: (a) 18.5 My model time as the back-arc reaches full crustal breakup; (b) 30 My model time, displaying back-arc spreading and fast trench-retreat. For the meaning of material colors see the legend of Figure 2. The red lines show the 420, 550, 900, and 1330°C isotherms. The gray arrows represent advection velocities (lengths scale with velocities).

the side boundaries are closed. At the base of the model, a free-slip condition is imposed and there is no material-transport through this boundary. In order to restrict the effects of the slab's interference with the bottom boundary of the model, the slab is transformed into lower mantle material at 1,200 km depth. The use of the arbitrary Lagrangian-Eulerian grid-setup allows for a free surface at the top of the model.

3. Results

We present four numerical experiments that explore how the relative rate of slab-pull build-up and overriding-plate weakening affect the style of back-arc rifting. Model 1 and Model 2 are end members in terms of the observed behavior from a set of 5 models, where we varied only the subducting plate velocity (see Supplementary animations in Supporting Information S2 for models with intermediate subducting plate velocities). Models 3 and 4 are identical to Model 2, but the oceanic basin has a finite width, a setup characteristic to Mediterranean style subduction systems.

3.1. Model 1—Reference Model

Model 1 is characterized by a v_{conv} = 5 cm yr^{-1} subducting plate velocity and no incoming pro-continental lithosphere (Figure 3; see supporting animation 1 in Supporting Information S2 for full model evolution). The weak mantle-lithosphere of the overriding plate starts thinning convectively and through ablative subduction erosion right from initiation of subduction. When the slab has reached 420 km depth around 8 My model time extension starts in the entire weak back-arc portion of the overriding plate. This phase of pure-shear style extension, accompanied by rapid trench-retreat stalls at around 10.4 My model time, as the tip of the slab reaches the 660 km

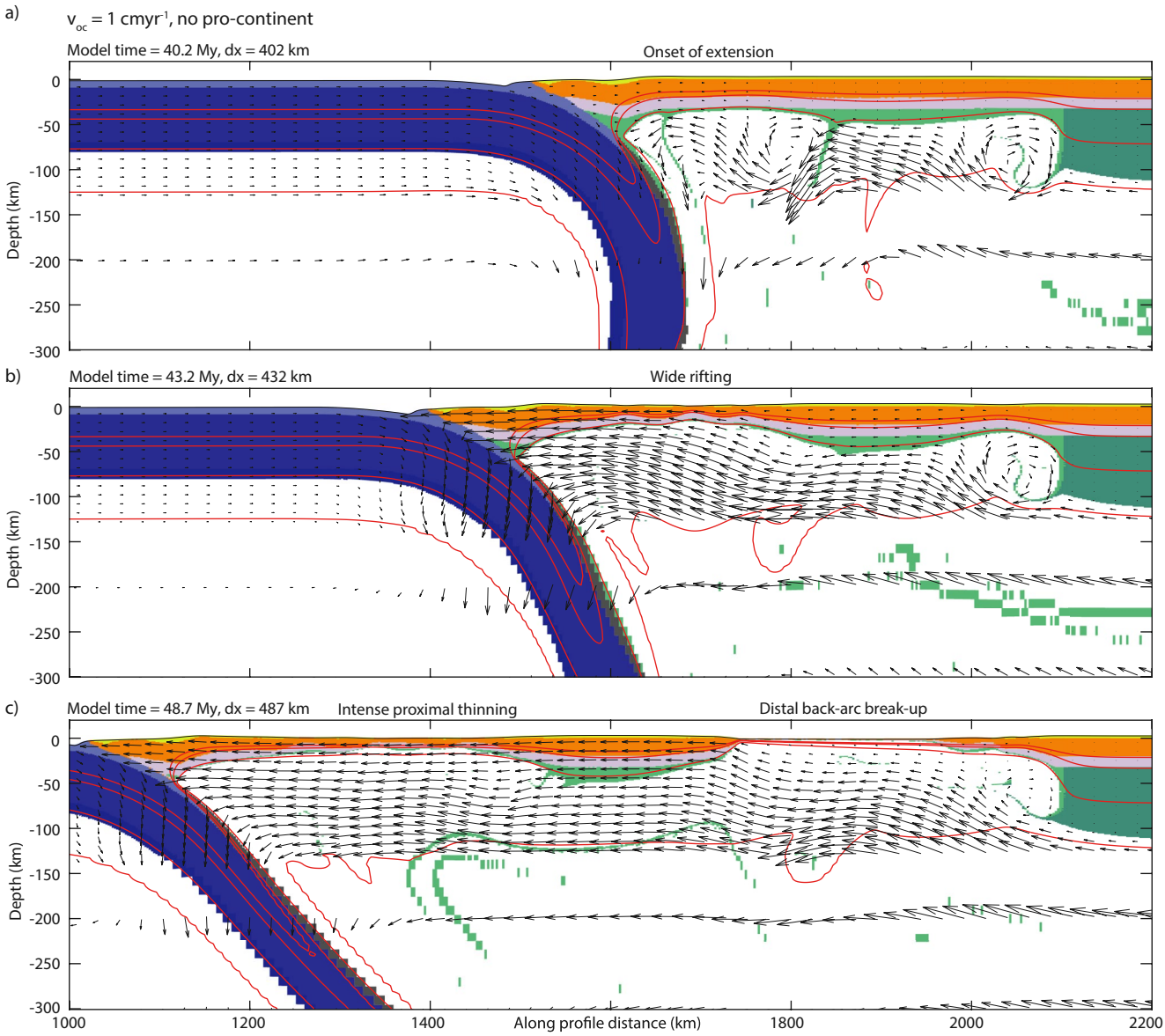

Figure 4. Results of Model 2. Panels (a–c) show zoomed-in images of the experiment's material domain at key time-steps: (a) after 40.2 My model time, when back-arc extension starts; (b) after 43.2 My when the boudinage style wide rifting of the proximal portion of the weak back-arc zone is most pronounced; (c) after 48.7 My when the back-arc reaches full crustal breakup at the distal portion of the weak back-arc zone. For the meaning of material colors see the legend of Figure 2. The red lines show the 420, 550, 900, and 1330°C isotherms. The gray arrows represent advection velocities (lengths scale with velocities).

phase transition zone. Extension starts again at around 15 My model time accompanied by slowly accelerating trench-retreat until the overriding plate reaches full crustal break-up at 18.5 My model time (Figure 3a). The resulting back-arc rift is narrow, symmetric, and separates an approximately 150 km wide lithospheric block from the rest of the overriding plate. From this point on, the rate of trench-retreat quickly reaches its peak value of 2.5 cm yr^{-1} with which the slab rolls back for the remainder of the model experiment (Figure 3b) leaving a stable spreading-center behind the arc.

3.2. Model 2—Slow Convergence

Model 2 is characterized by a subducting plate velocity of v_{conv} = 1 cm yr^{-1} and no incoming pro-continental lithosphere (Figure 4; supporting animation 2 in Supporting Information S2). Similarly, to Model 1, the weak

mantle-lithosphere of the overriding plate is convectively thinned following subduction initiation. However, as the velocity of the oceanic plate is 5 times lower compared to Model 1, there is almost no ablative removal of the overriding plate mantle lithosphere (Figure 4a). At this slower subducting plate velocity the slab reaches 400 km depth only after 40 My (Figure 4a). Convective removal of the weak portion of the back-arc mantle-lithosphere, however, occurs at the same timescale as in Model 1 leading to significant mantle thinning and associated crustal heating well before 39.5 My when extension of the overriding plate initiates (Figure 4a). From this point on, trench-retreat quickly reaches a maximum velocity of approximately 6.5 cm yr^{-1}, while the back-arc extends, resulting in a wide, asymmetric rift zone (Figure 4b). There are two main zones of extension and subsidence. A zone proximal to subduction trench exhibits boudinage style deformation and opens several small sub-basins. Subsequently extension shifts to the distal portion of the weak back-arc, where crustal break-up occurs around 48.7 My model time (Figure 4c).

3.3. Model 3—Pro-Continent, Narrow Ocean

Model 3 is characterized by subducting plate velocity of v_{conv} = 1 cm yr^{-1} and a narrow 450 km wide oceanic basin, flanked by the incoming pro-continental lithosphere (Figure 5; supporting animation 3 in Supporting Information S2). This model is designed to explore the behavior of Mediterranean style back-arc basins that are characterized by narrow, landlocked oceanic basins such as the Pannonian basin and a low subducting plate velocity, consistent with the relative velocity of Africa and Eurasia.

Similarly, to model 2, the convective removal of the weak portion of the overriding plate's mantle lithosphere starts after subduction initiation. Extension of the overriding plate lithosphere starts after 35 My model time (Figure 5a) and concentrates mainly in the proximal portion of the weak overriding plate lithosphere. The rate of trench-retreat progressively increases, and the two continental blocks collide at 39 My at which point the subducting plate velocity is set to v_{conv} = 0 cm yr^{-1} to mimic a soft docking. Nevertheless, the overriding plate continues extending, and by 40 My model time, a mildly asymmetric back-arc rift is formed approximately 250 km behind the suture zone (Figure 5b). This phase with decelerating extension stops as the slab detaches from the suture at 45.5 My model time, at which time the overriding plate exhibits approximately 125 km extension (Figure 5c).

For Model 3, we have calculated crustal and mantle lithospheric thinning factors before back-arc break-up and plotted the evolution of the topography in the proximal back-arc region (Figures 6a–6c). Back-arc extension is characterized by high mantle-lithospheric thinning factors and relatively low crustal thinning factors. The topographic evolution shows that the wide rift-zone located behind the subduction zone is a result of the progressive opening of a series of extensional sub-basins. The progression of the opening of these basins is trenchward, with the oldest basin the furthest and the youngest basin the closest to the subduction zone.

3.4. Model 4—Pro-Continent, Very Narrow Oceanic Basin

Model 4 is characterized by a subduction plate velocity of v_{conv} = 1 cm yr^{-1} and a 400 km wide oceanic basin, flanked by the incoming pro-continental lithosphere (Figure 7; supporting animation 4 in Supporting Information S2). This model is designed to explore what happens at the limit where the oceanic basin is not wide enough to generate sufficient slab-pull to drive the overriding plate into full lithospheric breakup.

The weak mantle lithosphere of the overriding plate behaves similarly to the previous two models and is thinned by convective removal after initiation of subduction. Trench-retreat and extension of the weakened overriding plate lithosphere start at around 34 My model time. The rate of extension increases rapidly with the velocity of trench-retreat with the latter reaching a maximum value of 2.6 cm yr^{-1} (at approximately 38 My model time) before the subducting plate velocity is set to v_{conv} = 0 cm yr^{-1} at 39 My. As in Model 3, the overriding plate continues to extend for a further 3.5 Mys (until approximately 42.5 My) albeit at a decelerating pace (Figure 7a) before the slab detaches, at around 51 My model time (Figure 7b).

The extension of the back-arc is focused to the proximal portion of the weak zone and results in a zone (approximately 200 km) of thinned crust and highly thinned mantle lithosphere. The overall trench-retreat is approximately 100 km.

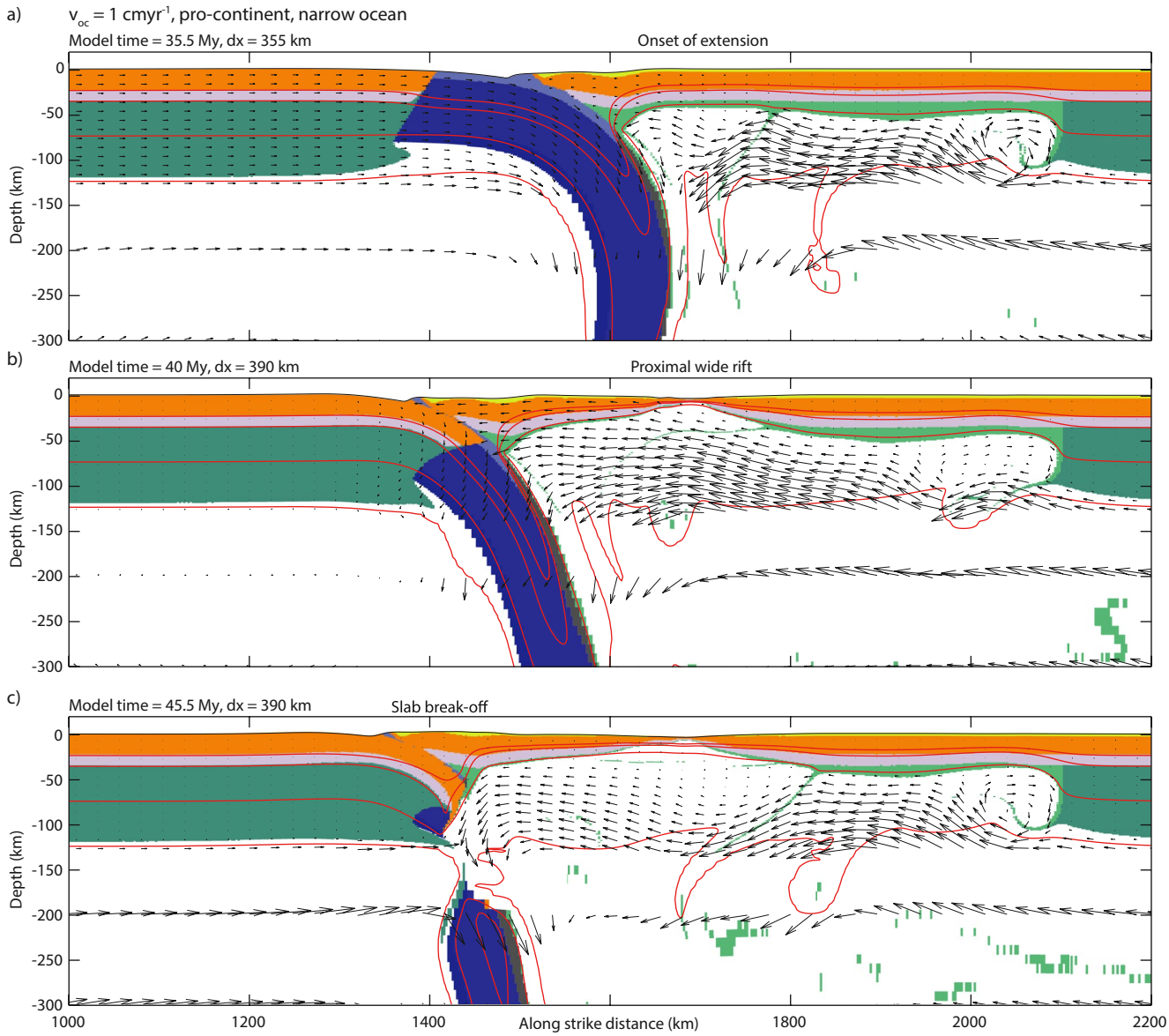

Figure 5. Results of Model 3. Panels (a–c) show zoomed-in images of the experiment's material domain at key time-steps: (a) after 35.5 My model time, when back-arc extension starts; (b) after 40 My model time, when the back-arc reaches full crustal breakup at; (c) 45.5 My model time, when the slab breaks off of the trailing continent after its soft docking at 39 My. For the meaning of material colors see the legend of Figure 2. The red lines show the 420, 550, 900, and 1330°C isotherms. The gray arrows represent advection velocities (lengths scale with velocities).

4. Discussion

4.1. Balance Between Slab-Pull and Back-Arc Thermal Regime

Models 1 and 2 both reach full crustal breakup, but the style of extension observed in the overriding plate is markedly different. The evolution of these systems can be understood through the balance of the main driving and resisting forces acting on the overriding plate lithosphere. The main driving force is the slab-pull that acts against the main resisting force that is the integrated strength of the overriding plate lithosphere. In addition to the strength of the lithosphere, resisting forces that act to dissipate the slab-pull force in the system include shear resistance along the subduction interface, bending resistance of the slab and viscous drag along the surface of the slab and along the base of the lithosphere. These additional dissipating mechanisms are largely unchanged between the models presented here and do not contribute to the contrasting behavior observed in the models presented here

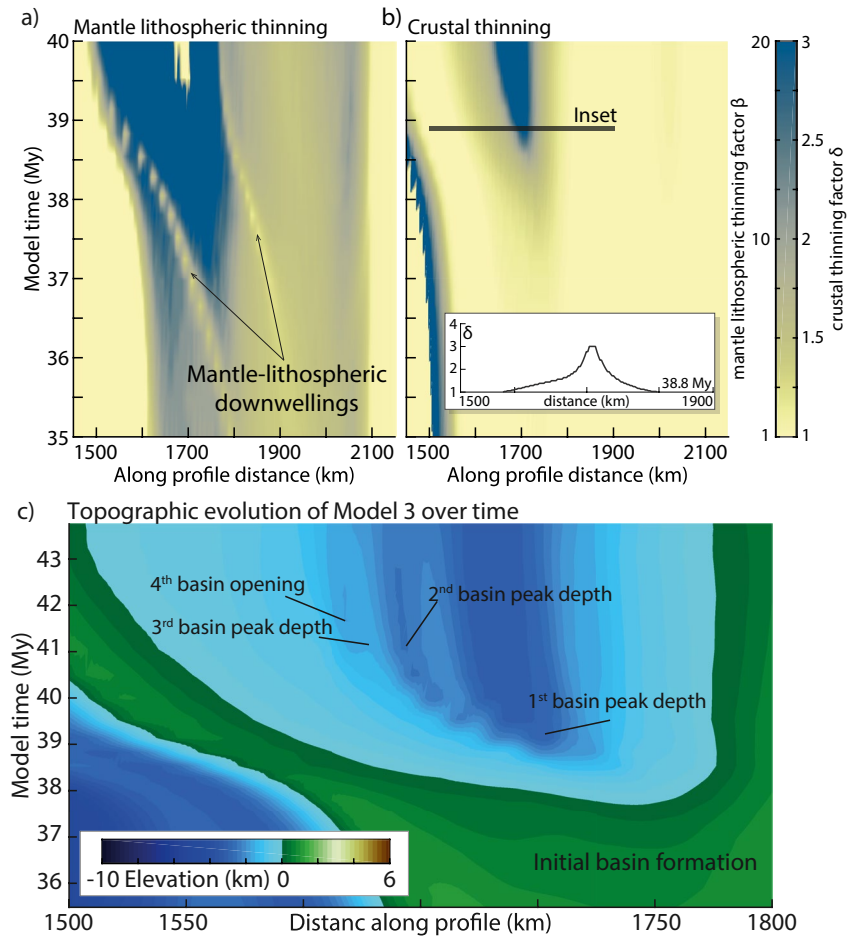

Figure 6. The time-evolution of (a) Mantle lithospheric and (b) Crustal stretching factors calculated for the weak portion of the back-arc of Model 4. Intensive crustal thinning starts at approximately 38 My model time, while break-up is reached at 40 My. Inset showing crustal thinning factors along a shorter transect at 38.8 My model time (transect marked with a gray line on panel b). (c) Late-stage topographic evolution of the back-arc portion of Model 3 over time. The sequence of back-arc basin openings is marked on the figure.

(for a detailed treatment of these forces we refer to Wolf and Huismans [2019] and Erdős et al. [2021]), hence we will focus here on the evolving balance of slab-pull and back-arc strength.

In case of Model 1, extension starts early and after a temporary stalling, the model reaches crustal breakup by 18 My model time (see Figure 8). As the subducting plate velocity is high, subduction of a long, relatively cold slab and associated slab-pull are established within 8–10 My (Figure 8a). At this time, the back-arc mantle-lithosphere is only moderately thinned and weakened and its overlying crust and upper mantle lithosphere remains cold and strong. In particular, the thickness and thermo-rheological structure of the crustal portion remains undisturbed with an average Moho-depth of 36 km and an average Moho-temperature of 550°C at the onset of extension. This combination of high slab-pull force and comparatively high back-arc strength results in the formation of a narrow rift-basin following a relatively small amount (approximately 125 km) of crustal extension.

In case of model 2, the low subducting plate velocity results in slow subduction with a slab that has more time to heat up. As a result, build-up of the associated slab-pull force takes more time and reaches a lower maximum value (Figure 8a). At the same time, convective thinning of the back-arc mantle-lithosphere and significant thermal weakening of the overlying crust occur before a long, upper mantle scale slab has been established. When finally slab-pull is sufficient to cause crustal extension in the overriding plate around 39.5 My, the Moho temperature locally reaches 850°C, with an average Moho temperature of approximately 755°C in the weak portion of the back-arc (Figure 4a), favoring ductile deformation and the formation of a very wide back-arc rift with approx-

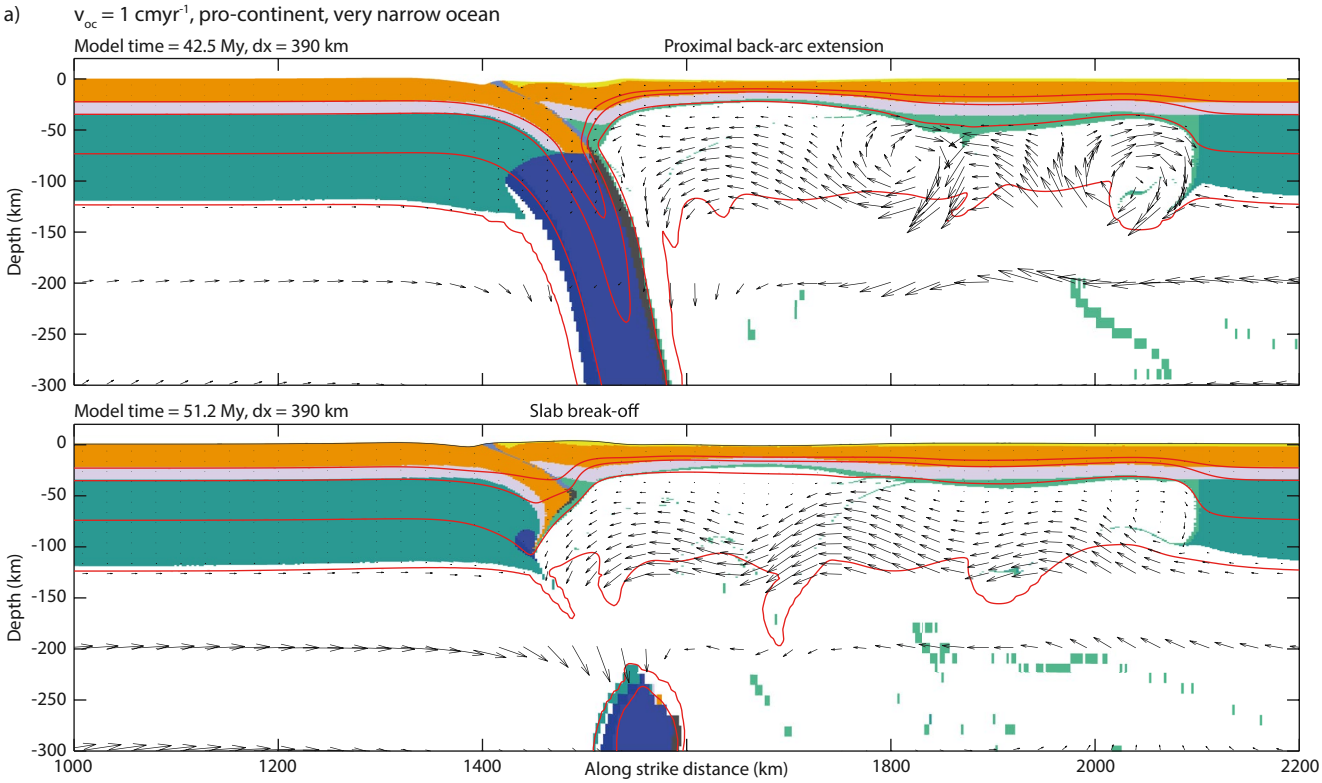

Figure 7. Results of Model 4. Panels (a and b) zoomed-in images of the experiment's material domain at key time-steps: (a) after 42.5 My model time, when back-arc extension ceases; (b) after 51.2 My model time when the slab breaks off. For the meaning of material colors see the legend of Figure 2. The red lines show the 420, 550, 900, and 1330°C isotherms. The gray arrows represent advection velocities (lengths scale with velocities).

imately 300 km of extension before lithospheric rupture. These high Moho temperature values are similar to those reported from extending continental back-arcs such as the Cascadia (e.g., Hyndman et al., 2005).

Sensitivity tests with subducting plate velocities between the presented endmember models 1 and 2 (Supplementary models S1–S6 in Supporting Information S2) show that the transition between the narrow and wide rifting modes occurs at very low (less than 1.5 cm yr^{-1}) subducting plate velocities. We have calculated characteristic timescales to describe the subduction (the time it takes for the slab to reach 400 km length) and the convective thinning (the time it takes to thin the overriding plate mantle-lithosphere to half of its original thickness) for all the models with varying subducting plate velocities. We have also calculated the pre-rift minimum back-arc strength at the start of extension and its ratio to the initial back-arc strength and plotted these values against the ratio of the two characteristic timescales (Figure 9). When the characteristic timescale of subduction is comparable to that of convective thinning (i.e., at high convergence rates) the ratio of pre-rift and initial back-arc strength is closer to 1, favoring a narrow back-arc rifting mode. Conversely, when the characteristic timescale of subduction is higher than that of convective thinning (i.e., at lower subducting plate velocities) the ratio of pre-rift and initial back-arc strength is low, favoring a wide back-arc rifting mode. A transition between these modes is tentatively marked on Figure 9 with a black dashed line.

It must be noted that the transition between these modes can be influenced by changes in other factors than the subduction plate velocity. In particular, the 600°C and higher Moho-temperatures are characteristic for all presented models with a slower convergence rate (up to 2 cm yr^{-1}). As granite melting starts at around 650°C these locally high Moho-temperatures would cause widespread partial melting which would result in lithospheric strength reduction. This additional melt weakening implies that the mode-change from narrow to wide rifting may occur already at higher subducting plate velocities. The transition is also dependent on the initial crustal thickness as well as crustal rheology, as thicker initial crust or a weaker quartz rheology would also promote a mode-transition at higher subducting plate velocities.

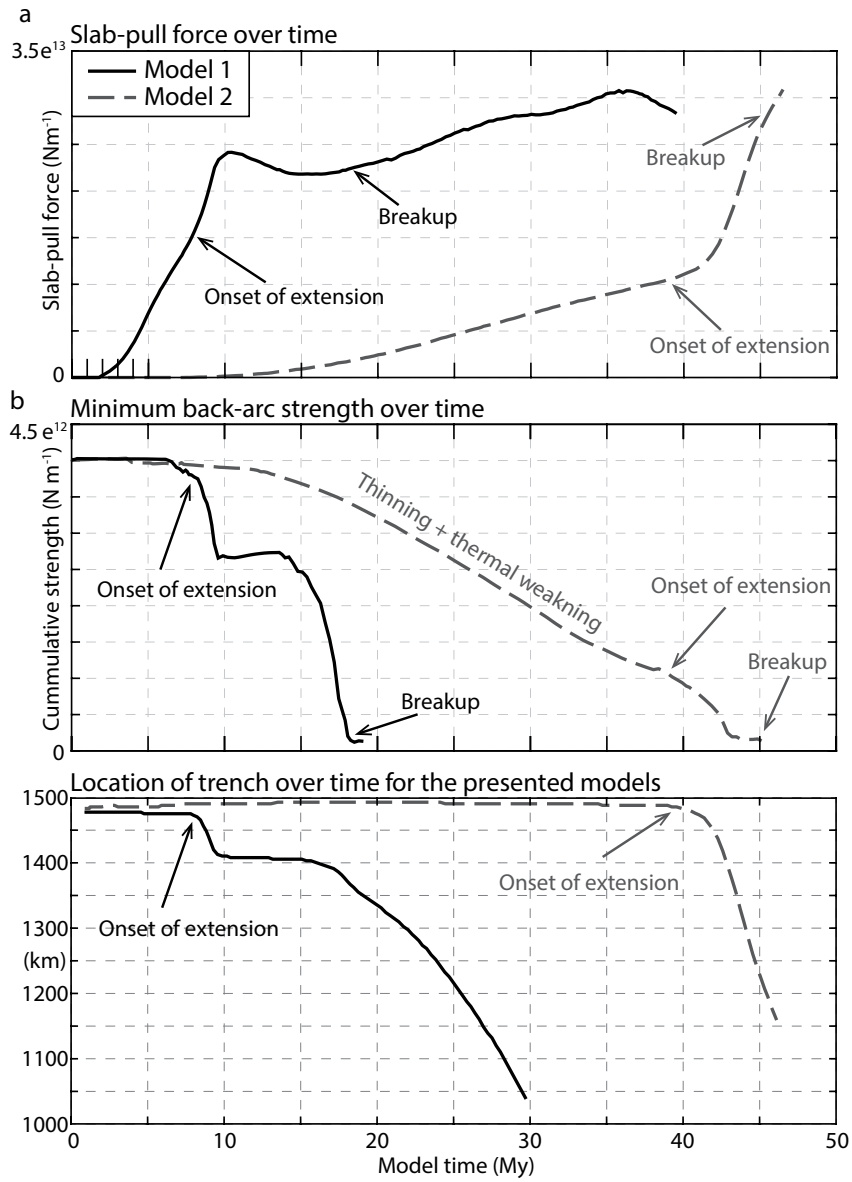

Figure 8. (a) Slab-pull force, (b) minimum back-arc strength, and (c) location of the trench over time for models 1 and 2, with key events marked for both models.

The contrasting behavior of models 1 and 2 shows that the relative timescales and co-evolution of (a) build-up of the slab-pull force through oceanic subduction and (b) back-arc weakening through convective thinning of the mantle-lithosphere and associated thermal weakening of the crust are the primary factors controlling the mode of extension in the overriding plate. In cases where the back-arc lithosphere is only moderately weakened by the time slab-pull is sufficient to overcome its strength, localized deformation is promoted resulting in a narrow back-arc rifting mode (Figure 10a). In turn, if the overriding plate is significantly weakened before sufficient slab-pull is established deformation is distributed resulting in a wide back-arc rifting mode (Figure 10b).

We next consider if varying trench-retreat velocity and strain-rate in the overriding plate affect the mode of back-arc extension in these models. Models 1 and 2 show highly different trench-retreat velocities, once back-arc extension is established (Figure 8c). Model 1 exhibits a low trench-retreat velocity with a peak value of 2.5 cm yr^{-1}. Back-arc extension in this model is established in a narrow rift mode. In contrast Model 2 has a peak trench-retreat velocity of 6.5 cm yr^{-1} and exhibits a wide rift mode of back-arc extension. Previous studies have suggested that low strain-rate and rheologically weak lithosphere promote wide rifting (e.g., Buck et al., 1999). In

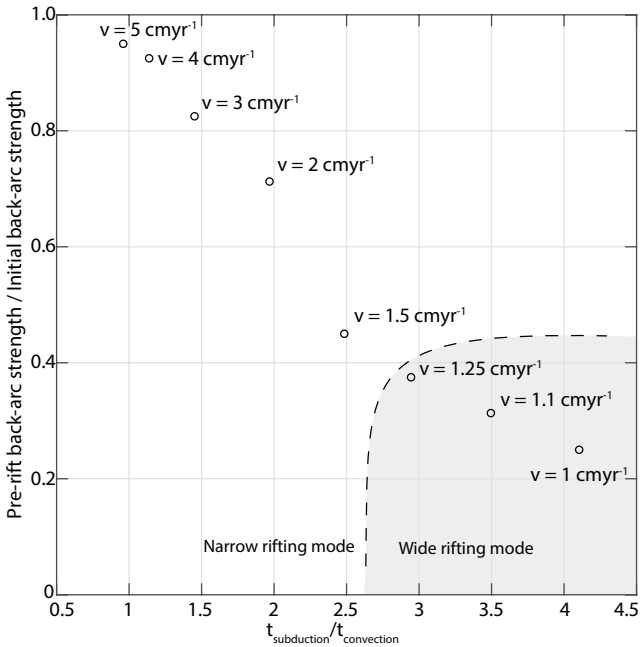

Figure 9. Mode selection plot. For details, see the discussion.

these models low strain-rate does not correlate with wide rifting. In contrast, the results suggest that the strength of the overriding plate lithosphere provides the dominant control on the mode of back-arc extension.

Comparing Models 2–4 show, that the size of the oceanic basin can be a strong limiting factor on the scale of back-arc extension. Model 3 shows that a 450 km wide oceanic basin can still be enough to produce back-arc breakup, but the amount of crustal extension (pre- as well as post-breakup) is severely limited. Model 4 (Figure 7) shows the system at its limit. The oceanic basin is too narrow to allow for sufficient slab rollback and for the build-up of a sufficiently high slab-pull force to overcome the strength of the overriding plate before the basin is closed. The result is a heavily thinned and extended back-arc lithosphere and an aborted rift. In our experimental setup a system with an oceanic basin less than 400 km wide is insufficient to produce a large enough slab-pull force that can result in overriding plate extension.

5. Comparison With the Pannonian Basin

The Pannonian basin is a wide, extensional basin in a back-arc position, floored by a very thin continental lithosphere (Figure 1). It was formed during the rapid rollback of the Carpathian slab between 20 Ma and 9 Ma, but its overall evolution was also affected by the Dinaric subduction (e.g., Balázs et al., 2016; Csontos et al., 1992; Fodor et al., 1999; Horváth et al., 2006; Matenco & Radivojević, 2012; Schmid et al., 2008). The slab imaged through seismic tomography below the East Carpathian Vrancea zone is approximately 450–500 km long (e.g., Martin et al., 2006; Wortel & Spakman, 2000) consistent with the small oceanic basin used in models 4 and 5. The 11 My time frame estimated for the back-arc extension is comparable to the time needed in our model experiments to get from initial crustal extension to continental breakup.

Neogene back-arc extension was preceded by an orogenic phase that resulted from the closure of the Neotethyan and the Alpine Tethyan oceanic realms (Csontos & Vörös, 2004; Handy et al., 2010; Schmid et al., 2008). During this complex history of oceanic closures and collisions, three distinct terrains (ALCAPA, Tisza and Dacia) experienced episodes of collision and thickening before getting juxtaposed. Consequently, they could have had a weaker rheological setup than their surroundings, including the chance of a much-weakened mantle lithospheric root such as the one employed in our experiments.

An estimated 150–200 km extension has taken place in the Pannonian basin and the associated crustal thinning factors are in the order of 1.5–2.2 (Horváth et al., 2006; Lenkey, 1999). Moreover, most data points to extremely high (locally reaching up to 5–20) mantle lithosphere thinning factors (Horváth et al., 2006; Lenkey, 1999; Sclater et al., 1980). In our preferred experiment (Model 3), the amount of trench-retreat prior to crustal break-up is approximately 125 km, although the trench did retreat a further 50 km continuing even after the collision had started. The mantle lithospheric thinning factors prior crustal breakup are generally in the order of 5–20 (Figure 6), although close to the proximal rift basin they locally exceed these values. In turn, the crust remains practically intact until about 2 My before break-up. From this onset, the crustal thinning is focused on an approximately 200 km wide region (necking zone) and the crustal thinning factor gradually increases to around 3 about 1 My prior break-up (Figure 6).

The surface heat flow density distribution in the Pannonian basin shows values ranging from 50 to 130 mWm^{-2}, with a mean value of 100 mWm^{-2} (Lenkey et al., 2002). In our preferred experiment, just prior crustal break-up the surface heat flow density values are within this range, with values approaching 120 mWm^{-2} around the necking zone while in the rest of the weak back-arc they are slightly elevated from a background value of 52 mWm^{-2} to around 58–62 mWm^{-2}.

It must be noted that the late-stage alkaline volcanism and various basin modeling studies suggest that significant mantle thinning occurred at a later stage of rifting in the Pannonian basin, and it does not precede rifting, although there is no strong evidence as to when mantle-lithospheric thinning started (e.g., Harangi et al., 2014; Horváth

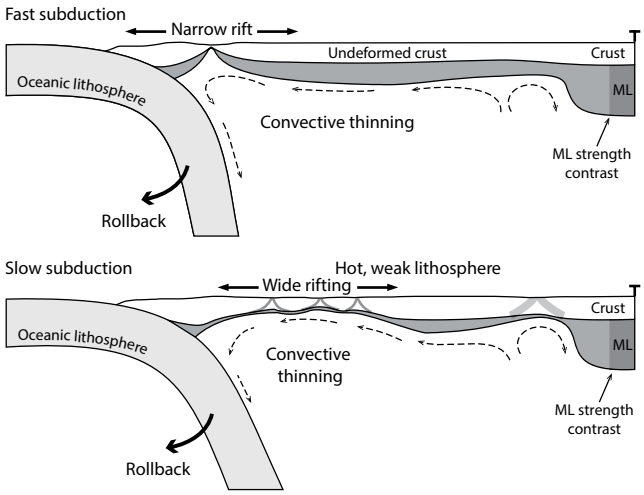

Figure 10. Generalized cartoons of the presented key models showing the effect of varying subducting plate velocity combined with a weak overriding plate lithosphere. Panel (a) shows the narrow rifting style resulting from high subducting plate velocity (corresponding to Model 1) while panel (b) shows the wide rifting style resulting from low subducting plate velocity (corresponding to Model 2).

et al., 2015; Huismans et al., 2001; Royden et al., 1983; Tiliţă et al., 2013). This observation contrasts with our models where convective removal of the mantle-lithosphere occurs before rifting. Therefore, we cannot rule out that other factors aided in weakening the Pannonian crust such as previously overthickened crust or an inherently weak quartz rheology allowing for the observed wide extension.

Naturally, the 3D nature of the Pannonian basin—with the Dinaric slab retreating at its south-western edge and the lithospheric scale extrusion from the Eastern Alps—resulted in a much more complex spatiotemporal basin evolution including an enigmatic short-lived Sarmatian inversion phase (see Balázs et al., 2016 and references therein). Nevertheless, subduction appears to be present only under the East Carpathians and as peak deformation in the Dinarides and the Eastern Alps predates that of the Pannonian basin (e.g., Ustaszewski et al., 2008) most of the extension (from the Oligocene—Early Miocene onwards) likely resulted from the eastward retreat of the Carpathian Slab. The overall E-W direction of back-arc extension and the well-established mantle lithosphere thinning beneath the Pannonian back-arc basin allow first order comparison with the 2D models presented here.

Furthermore, the presence of the Transylvanian basin and the Apuseni mountains with their comparatively thicker lithospheric roots imaged through seismic tomography (Dérerová et al., 2006) between the Pannonian basin and the East Carpathians further complicates the geological setup. However, in a previous modeling study we have shown that tensional back-arc stresses can be transmitted through a stronger block akin to the Transylvanian basin to cause widespread extension in a region characterized by a weaker lithospheric structure (Erdős et al., 2021).

The deformation pattern observed in Model 4 corresponds well to that observed in the Pannonian basin. In the Pannonian basin, extension could locally concentrate in discrete zones where pull-apart basins developed (Balázs et al., 2016; Csontos et al., 1992; Fodor et al., 1999; Horváth, 1993). The heterogeneity of extension is also reflected in the variation of pre-Neogene basement depth; elevated basement blocks separate deep sub-basins where the thickness of the Neogene-Quaternary sedimentary rocks can reach 6–7 km (Horváth et al., 2006).

In Model 4, the style of rifting is rather wide, with a number of distinct sub-basins distributed along the back-arc. Chronologically, the first basin to form in a back-arc position is a sag-basin approximately 150 km behind the trench. Its origin is analogous to that suggested for the Transylvanian basin; a continental sag caused by the suction force exerted to the upper plate by the down bending Carpathian slab (Horváth et al., 2006; Royden et al., 1982).

After the onset of back-arc rifting, basin formation shifts about 300 km behind the trench. The wide depression forming above the extending crust progressively breaks up into 4 sub-basins, with each new basin separated from the next by a basement high (Figure 6). Each new basin forms closer to the trench than the previous one, but they are progressively shallower as well, with the oldest basin reaching 4 km maximum depth, while the youngest only 1.8 km (Figure 6). These extensional basins are separated from the sag basin by a pronounced topographic high of about 50 km width which corresponds well to the Apuseni mountains separating the Great Hungarian Plain from the Transylvanian basin.

6. Conclusions

We have used 2D numerical models to study the delicate interplay between subducting plate velocity and back-arc weakening.

Our results suggest that the balance between the build-up of slab-pull and the weakening of the overriding plate through the convective thinning of its mantle-lithosphere and the thermal weakening of its crust plays a crucial role in determining the style of back-arc extension. When the subducting plate velocity is high, slab-pull builds up

fast, while the back-arc lithosphere remains relatively strong, resulting in a narrow rift-zone. When the subducting plate velocity is sufficiently low, the slab-pull builds up slowly and the back-arc lithosphere has a longer time to weaken, resulting in a wide rift zone. The velocity of trench-retreat plays a secondary role in determining the style of rifting compared to the rheology of the overriding plate at the time of rift initiation. The presence of a continental lithospheric block trailing the subducting oceanic basin also has a modulating effect on the deformation style of the overriding plate. Narrower oceanic basins produce less pre-breakup extension, although the effect is only second order. At the limit, subduction of a very narrow oceanic basin can result in significant back-arc extension without reaching full crustal breakup.

The modeling results reproduce well some of the first order features of the Pannonian basin such as the thin lithosphere, the inhomogeneous lithospheric thinning, the locally high surface heat flow values, the moderate amount of pre-breakup extension, and the wide, distributed extension in the back-arc basin.

Data Availability Statement

No new data were used for this study. Parameter values used to produce the numerical model results are provided in Table 1. Numerical models are computed with published methods and codes, described in Section 2 and Supporting Information S1. Model inputs and outputs, including plotting scripts is available at (https://doi.org/10.5281/zenodo.6368141).

Acknowledgments
This work has been carried out by the financial support of the Hungarian National Research Fund project OTKA-K120149. The authors thank Uninett Sigma2 for computing time of project NN4704K. The authors would like to thank Laurent Jolivet for his excellent editorial work as well as the three anonymous reviewers for their constructive comments.

References

Arcay, D., Doin, M. P., Tric, E., Bousquet, R., & de Capitani, C. (2006). Overriding plate thinning in subduction zones: Localized convection induced by slab dehydration. *Geochemistry, Geophysics, Geosystems*, *7*(2). https://doi.org/10.1029/2005gc001061

Arcay, D., Tric, E., & Doin, M. P. (2005). Numerical simulations of subduction zones. *Physics of the Earth and Planetary Interiors*, *149*(1–2), 133–153. https://doi.org/10.1016/j.pepi.2004.08.020

Bada, G., Horvath, F., Gerner, P., & Fejes, I. (1999). Review of the present-day geodynamics of the Pannonian basin: Progress and problems. *Journal of Geodynamics*, *27*(4–5), 501–527. https://doi.org/10.1016/S0264-3707(98)00013-1

Balázs, A., Burov, E., Matenco, L., Vogt, K., Francois, T., & Cloetingh, S. (2017). Symmetry during the syn- and post-rift evolution of extensional back-arc basins: The role of inherited orogenic structures. *Earth and Planetary Science Letters*, *462*, 86–98. https://doi.org/10.1016/j.epsl.2017.01.015

Balázs, A., Matenco, L., Magyar, I., Horváth, F., & Cloetingh, S. (2016). The link between tectonics and sedimentation in back-arc basins: New genetic constraints from the analysis of the Pannonian Basin. *Tectonics*, *35*(6), 1526–1559. https://doi.org/10.1002/2015tc004109

Bassi, G. (1995). Relative importance of strain rate and rheology for the mode of continental extension. *Geophysical Journal International*, *122*(1), 195–210. https://doi.org/10.1111/j.1365-246X.1995.tb03547.x

Beaumont, C., Nguyen, M. H., Jamieson, R. A., & Ellis, S. (2006). Crustal flow modes in large hot orogens. *Geological Society, London, Special Publications*, *268*(1), 91–145. https://doi.org/10.1144/gsl.sp.2006.268.01.05

Behr, W. M., & Becker, T. W. (2018). Sediment control on subduction plate speeds. *Earth and Planetary Science Letters*, *502*, 166–173. https://doi.org/10.1016/j.epsl.2018.08.057

Billen, M. I. (2010). Slab dynamics in the transition zone. *Physics of the Earth and Planetary Interiors*, *183*(1–2), 296–308. https://doi.org/10.1016/j.pepi.2010.05.005

Brun, J. P. (1999). Narrow rifts versus wide rifts: Inferences for the mechanics of rifting from laboratory experiments. *Philosophical Transactions of the Royal Society of London, Series A: Mathematical, Physical and Engineering Sciences*, *357*(1753), 695–712. https://doi.org/10.1098/rsta.1999.0349

Buck, W. R. (1991). Modes of continental lithospheric extension. *Journal of Geophysical Research: Solid Earth*, *96*(B12), 20161–20178. https://doi.org/10.1029/91jb01485

Buck, W. R., Lavier, L. L., & Poliakov, A. (1999). How to make a rift wide. *Philosophical Transactions of the Royal Society A: Mathematical, Physical & Engineering Sciences*, *357*(1753), 671–693. https://doi.org/10.1098/rsta.1999.0348

Buiter, S. J. H., Huismans, R. S., & Beaumont, C. (2008). Dissipation analysis as a guide to mode selection during crustal extension and implications for the styles of sedimentary basins. *Journal of Geophysical Research*, *113*(B6), B06406. https://doi.org/10.1029/2007jb005272

Burov, E. (2007). The role of gravitational instabilities, density structure and extension rate in the evolution of continental margins. *Geological Society, London, Special Publications*, *282*(1), 139–156. https://doi.org/10.1144/sp282.7

Burov, E., & Poliakov, A. (2001). Erosion and rheology controls on synrift and postrift evolution: Verifying old and new ideas using a fully coupled numerical model. *Journal of Geophysical Research: Solid Earth*, *106*(B8), 16461–16481. https://doi.org/10.1029/2001jb000433

Chen, Z., Schellart, W. P., & Duarte, J. C. (2015). Overriding plate deformation and variability of fore-arc deformation during subduction: Insight from geodynamic models and application to the Calabria subduction zone. *Geochemistry, Geophysics, Geosystems*, *16*(10), 3697–3715. https://doi.org/10.1002/2015gc005958

Csontos, L., Nagymarosy, A., Horvath, F., & Kovac, M. (1992). Tertiary evolution of the Intra-Carpathian area: A model. *Tectonophysics*, *208*(1–3), 221–241. https://doi.org/10.1016/0040-1951(92)90346-8

Csontos, L., & Vörös, A. (2004). Mesozoic plate tectonic reconstruction of the Carpathian region. *Palaeogeography, Palaeoclimatology, Palaeoecology*, *210*, 1–56. https://doi.org/10.1016/j.palaeo.2004.02.033

Currie, C. A., Huismans, R. S., & Beaumont, C. (2008). Thinning of continental backarc lithosphere by flow-induced gravitational instability. *Earth and Planetary Science Letters*, *269*(3–4), 436–447. https://doi.org/10.1016/j.epsl.2008.02.037

Dérerová, J., Zeyen, H., Bielik, M., & Salman, K. (2006). Application of integrated geophysical modeling for determination of the continental lithospheric thermal structure in the eastern Carpathians. *Tectonics*, *25*(3). https://doi.org/10.1029/2005tc001883

Erdős, Z., Huismans, R. S., Faccenna, C., & Wolf, S. G. (2021). The role of subduction interface and upper plate strength on back-arc extension: Application to Mediterranean back-arc basins. *Tectonics*, *40*(8). https://doi.org/10.1029/2021tc006795

Faccenna, C., Becker, T. W., Auer, L., Billi, A., Boschi, L., Brun, J. P., et al. (2014). Mantle dynamics in the Mediterranean. *Reviews of Geophysics*, *52*(3), 283–332. https://doi.org/10.1002/2013rg000444

Faccenna, C., Heuret, A., Funiciello, F., Lallemand, S., & Becker, T. W. (2007). Predicting trench and plate motion from the dynamics of a strong slab. *Earth and Planetary Science Letters*, *257*(1–2), 29–36. https://doi.org/10.1016/j.epsl.2007.02.016

Faccenna, C., Mattei, M., Funiciello, F., & Jolivet, L. (1997). Styles of back-arc extension in the central Mediterranean. *Terra Nova*, *9*(3), 126–130. https://doi.org/10.1046/j.1365-3121.1997.d01-12.x

Fodor, L., Csontos, L., Bada, G., Györfi, I., & Benkovics, L. (1999). Tertiary tectonic evolution of the Pannonian Basin system and neighbouring orogens: A new synthesis of palaeostress data. *Geological Society, London, Special Publications*, *156*(1), 295–334. https://doi.org/10.1144/gsl.sp.1999.156.01.15

Funiciello, F., Morra, G., Regenauer-Lieb, K., & Giardini, D. (2003). Dynamics of retreating slabs: 1. Insights from two-dimensional numerical experiments. *Journal of Geophysical Research*, *108*(B4). https://doi.org/10.1029/2001jb000898

Gerya, T. V., & Meilick, F. I. (2011). Geodynamic regimes of subduction under an active margin: Effects of rheological weakening by fluids and melts. *Journal of Metamorphic Geology*, *29*(1), 7–31. https://doi.org/10.1111/j.1525-1314.2010.00904.x

Gleason, G. C., & Tullis, J. (1995). A flow law for dislocation creep of quartz aggregates determined with the molten-salt cell. *Tectonophysics*, *247*(1–4), 1–23. https://doi.org/10.1016/0040-1951(95)00011-B

Goes, S., Agrusta, R., van Hunen, J., & Garel, F. (2017). Subduction-transition zone interaction: A review. *Geosphere*, *13*(3), 644–664. https://doi.org/10.1130/Ges01476.1

Hacker, B. R. (1996). Eclogite formation and the rheology, buoyancy, seismicity, and H_2O content of oceanic crust. In G. E. Bebout, D. W. Scholl, S. H. Kirby, & J. P. Platt (Eds.), *Subduction top to bottom* (pp. 337–346).

Handy, M. R., Schmid, S. M., Bousquet, R., Kissling, E., & Bernoulli, D. (2010). Reconciling plate-tectonic reconstructions of Alpine Tethys with the geological–geophysical record of spreading and subduction in the Alps. *Earth-Science Reviews*, *102*(3–4), 121–158. https://doi.org/10.1016/j.earscirev.2010.06.002

Harangi, S., Jankovics, M. É., Sági, T., Kiss, B., Lukács, R., & Soós, I. (2014). Origin and geodynamic relationships of the Late Miocene to Quaternary alkaline basalt volcanism in the Pannonian basin, eastern–central Europe. *International Journal of Earth Sciences*, *104*(8), 2007–2032. https://doi.org/10.1007/s00531-014-1105-7

Heuret, A., Funiciello, F., Faccenna, C., & Lallemand, S. (2007). Plate kinematics, slab shape and back-arc stress: A comparison between laboratory models and current subduction zones. *Earth and Planetary Science Letters*, *256*(3–4), 473–483. https://doi.org/10.1016/j.epsl.2007.02.004

Heuret, A., & Lallemand, S. (2005). Plate motions, slab dynamics and back-arc deformation. *Physics of the Earth and Planetary Interiors*, *149*(1–2), 31–51. https://doi.org/10.1016/j.pepi.2004.08.022

Horváth, F. (1993). Towards a mechanical model for the formation of the Pannonian basin. *Tectonophysics*, *226*(1–4), 333–357. https://doi.org/10.1016/0040-1951(93)90126-5

Horváth, F., Bada, G., Szafián, P., Tari, G., Ádám, A., & Cloetingh, S. (2006). Formation and deformation of the Pannonian Basin: Constraints from observational data. In D. Gee & R. Stephenson (Eds.), *European lithospheric dynamics* (pp. 191–206). Geological Society.

Horváth, F., Musitz, B., Balázs, A., Végh, A., Uhrin, A., Nádor, A., et al. (2015). Evolution of the Pannonian basin and its geothermal resources. *Geothermics*, *53*, 328–352. https://doi.org/10.1016/j.geothermics.2014.07.009

Huismans, R. S., & Beaumont, C. (2003). Symmetric and asymmetric lithospheric extension: Relative effects of frictional-plastic and viscous strain softening. *Journal of Geophysical Research*, *108*(B10). https://doi.org/10.1029/2002jb002026

Huismans, R. S., & Beaumont, C. (2008). Complex rifted continental margins explained by dynamical models of depth-dependent lithospheric extension. *Geology*, *36*(2), 163. https://doi.org/10.1130/g24231a.1

Huismans, R. S., & Beaumont, C. (2011). Depth-dependent extension, two-stage breakup and cratonic underplating at rifted margins. *Nature*, *473*(7345), 74–78. https://doi.org/10.1038/nature09988

Huismans, R. S., Podladchikov, Y. Y., & Cloetingh, S. (2001). Dynamic modeling of the transition from passive to active rifting, application to the Pannonian basin. *Tectonics*, *20*(6), 1021–1039. https://doi.org/10.1029/2001tc900010

Hyndman, R. D., Currie, C. A., & Mazzotti, S. P. (2005). Subduction zone backarcs, mobile belts, and orogenic heat. *Geological Society of America Today*, *15*(2), 4. https://doi.org/10.1130/1052-5173(2005)015<4:SZBMBA>2.0.CO;2

Jolivet, L., Faccenna, C., D'Agostino, N., Fournier, M., & Worrall, D. (1999). The kinematics of back-arc basins, examples from the Tyrrhenian, Aegean and Japan Seas. In C. Mac Niocaill & P. D. Ryan (Eds.), *Continental tectonics* (pp. 21–53). Geological Society, Special Publications.

Karato, S., & Wu, P. (1993). Rheology of the upper mantle: A synthesis. *Science*, *260*(5109), 771–778. https://doi.org/10.1126/science.260.5109.771

Király, Á., Capitanio, F. A., Funiciello, F., & Faccenna, C. (2016). Subduction zone interaction: Controls on arcuate belts. *Geology*, *44*(9), 715–718. https://doi.org/10.1130/g37912.1

Lenkey, L. (1999). *Geothermics of the Pannonian basin and its bearing on the tectonics of basin evolution* (p. 215). Department of Sedimentary Geology, Faculty of Earth Sciences. Vrije Universiteit.

Lenkey, L., Dovenyi, P., Horvath, F., & Cloetingh, S. (2002). *Geothermics of the Pannonian basin and its bearing on the neotectonics* (Vol. 3, pp. 29–40). EGU Stephan Mueller Special Publication Series.

Liao, J., & Gerya, T. (2014). Influence of lithospheric mantle stratification on craton extension: Insight from two-dimensional thermo-mechanical modeling. *Tectonophysics*, *631*, 50–64. https://doi.org/10.1016/j.tecto.2014.01.020

Linzer, H. G., Frisch, W., Zweigel, P., Girbacea, R., Hann, H. P., & Moser, F. (1998). Kinematic evolution of the Romanian Carpathians. *Tectonophysics*, *297*(1–4), 133–156. https://doi.org/10.1016/s0040-1951(98)00166-8

Mackwell, S. J., Zimmerman, M. E., & Kohlstedt, D. L. (1998). High-temperature deformation of dry diabase with application to tectonics on Venus. *Journal of Geophysical Research*, *103*(B1), 975–984. https://doi.org/10.1029/97jb02671

Magni, V., Faccenna, C., van Hunen, J., & Funiciello, F. (2014). How collision triggers backarc extension: Insight into Mediterranean style of extension from 3-D numerical models. *Geology*, *42*(6), 511–514. https://doi.org/10.1130/g35446.1

Martin, M., & Wenzel, F., & CALIXTO Working Group. (2006). High-resolution teleseismic body wave tomography beneath SE-Romania - II. Imaging of a slab detachment scenario. *Geophysical Journal International*, *164*(3), 579–595. https://doi.org/10.1111/j.1365-246X.2006.02884.x

Matenco, L., Munteanu, I., ter Borgh, M., Stanica, A., Tilita, M., Lericolais, G., et al. (2016). The interplay between tectonics, sediment dynamics and gateways evolution in the Danube system from the Pannonian Basin to the western Black Sea. *The Science of the Total Environment*, *543*, 807–827. https://doi.org/10.1016/j.scitotenv.2015.10.081

Matenco, L., & Radivojević, D. (2012). On the formation and evolution of the Pannonian Basin: Constraints derived from the structure of the junction area between the Carpathians and Dinarides. *Tectonics*, *31*(6). https://doi.org/10.1029/2012tc003206

Mitrovica, J. X., & Forte, A. M. (2004). A new inference of mantle viscosity based upon joint inversion of convection and glacial isostatic adjustment data. *Earth and Planetary Science Letters*, *225*(1–2), 177–189. https://doi.org/10.1016/j.epsl.2004.06.005

Qi, J., Zhang, X., Wu, Z., Meng, X., Shang, L., Li, Y., et al. (2021). Characteristics of crustal variation and extensional break-up in the Western Pacific back-arc region based on a wide-angle seismic profile. *Geoscience Frontiers*, *12*(3), 101082. https://doi.org/10.1016/j.gsf.2020.09.011

Royden, L., Horváth, F., Nagymarosy, A., & Stegena, L. (1983). Evolution of the Pannonian basin system: 2. Subsidence and thermal history. *Tectonics*, *2*(1), 91–137. https://doi.org/10.1029/TC002i001p00091

Royden, L. H., Horvath, F., & Burchfiel, B. C. (1982). Transform faulting, extension, and subduction in the Carpathian Pannonian region. *The Geological Society of America Bulletin*, *93*(8), 717–725. https://doi.org/10.1130/0016-7606(1982)93<717:Tfeasi>2.0.Co;2

Schellart, W. P., Freeman, J., Stegman, D. R., Moresi, L., & May, D. (2007). Evolution and diversity of subduction zones controlled by slab width. *Nature*, *446*(7133), 308–311. https://doi.org/10.1038/nature05615

Schellart, W. P., & Moresi, L. (2013). A new driving mechanism for backarc extension and backarc shortening through slab sinking induced toroidal and poloidal mantle flow: Results from dynamic subduction models with an overriding plate. *Journal of Geophysical Research: Solid Earth*, *118*(6), 3221–3248. https://doi.org/10.1002/jgrb.50173

Schmid, S. M., Bernoulli, D., Fügenschuh, B., Matenco, L., Schefer, S., Schuster, R., et al. (2008). The Alpine-Carpathian-Dinaridic orogenic system: Correlation and evolution of tectonic units. *Swiss Journal of Geosciences*, *101*(1), 139–183. https://doi.org/10.1007/s00015-008-1247-3

Sclater, J. G., Royden, L., Horváth, F., Burchfiel, B. C., Semken, S., & Stegena, L. (1980). The Formation of the intra-Carpathian basins as determined from subsidence data. *Earth and Planetary Science Letters*, *51*(1), 139–162. https://doi.org/10.1016/0012-821x(80)90262-9

Sdrolias, M., & Müller, R. D. (2006). Controls on back-arc basin formation. *Geochemistry, Geophysics, Geosystems*, *7*(4). https://doi.org/10.1029/2005gc001090

Shemenda, A. I. (1993). Subduction of the lithosphere and back arc dynamics: Insights from physical modeling. *Journal of Geophysical Research*, *98*(B9), 16167. https://doi.org/10.1029/93jb01094

Sheng, J., Li, C., Liao, J., Yang, Z., Jiang, S., & Li, S. (2018). Dynamics of back-arc extension controlled by subducting slab retreat: Insights from 2D thermo-mechanical modelling. *Geological Journal*, *10*(6), 3376–3388. https://doi.org/10.1002/gj.3336

Sibuet, J. C., Deffontaines, B., Hsu, S. K., Thareau, N., Le Formal, J. P., Liu, C. S., & Party, A. (1998). Okinawa trough backarc basin: Early tectonic and magmatic evolution. *Journal of Geophysical Research*, *103*(B12), 30245–30267. https://doi.org/10.1029/98jb01823

Sibuet, J. C., Letouzey, J., Barbier, F., Charvet, J., Foucher, J. P., Hilde, T. W. C., et al. (1987). Back arc extension in the Okinawa Trough. *Journal of Geophysical Research*, *92*(B13), 14041–14063. https://doi.org/10.1029/JB092iB13p14041

Sperner, B., Ratschbacher, L., & Nemčok, M. (2002). Interplay between subduction retreat and lateral extrusion: Tectonics of the Western Carpathians. *Tectonics*, *21*(6), 1–24. https://doi.org/10.1029/2001TC901028

Tamaki, K. (1985). Two modes of back-arc spreading. *Geology*, *13*(7), 475. https://doi.org/10.1130/0091-7613(1985)13<475:Tmobs>2.0.Co;2

Taylor, B., & Karner, G. D. (1983). On the evolution of marginal basins. *Reviews of Geophysics*, *21*(8), 1727. https://doi.org/10.1029/RG021i008p01727

Thieulot, C. (2011). FANTOM: Two- and three-dimensional numerical modelling of creeping flows for the solution of geological problems. *Physics of the Earth and Planetary Interiors*, *188*(1–2), 47–68. https://doi.org/10.1016/j.pepi.2011.06.011

Tiliţă, M., Matenco, L., Dinu, C., Ionescu, L., & Cloetingh, S. (2013). Understanding the kinematic evolution and genesis of a back-arc continental "sag" basin: The Neogene evolution of the Transylvanian Basin. *Tectonophysics*, *602*, 237–258. https://doi.org/10.1016/j.tecto.2012.12.029

Ustaszewski, K., Schmid, S. M., Fügenschuh, B., Tischler, M., Kissling, E., & Spakman, W. (2008). A map-view restoration of the Alpine-Carpathian-Dinaridic system for the Early Miocene. *Swiss Journal of Geosciences*, *101*(S1), 273–294. https://doi.org/10.1007/s00015-008-1288-7

Wolf, S. G., & Huismans, R. S. (2019). Mountain building or backarc extension in ocean-continent subduction systems: A function of backarc lithospheric strength and absolute plate velocities. *Journal of Geophysical Research: Solid Earth*, *124*(7), 7461–7482. https://doi.org/10.1029/2018jb017171

Wortel, M. J., & Spakman, W. (2000). Subduction and slab detachment in the Mediterranean-Carpathian region. *Science*, *290*(5498), 1910–1917. https://doi.org/10.1126/science.290.5498.1910

Zhang, Y., Gaetani, G., Zeng, Z., Monteleone, B., Yin, X., Wang, X., & Chen, S. (2021). Halogen (F, Cl) concentrations and Sr-Nd-Pb-B isotopes of the basaltic andesites from the southern Okinawa Trough: Implications for the recycling of subducted serpentinites. *Journal of Geophysical Research: Solid Earth*, *126*(3). https://doi.org/10.1029/2021jb021709